nature

https://doi.org/10.1038/s41586-022-04441-6

Accelerated Article Preview

SARS-CoV-2 Omicron virus causes attenuated disease in mice and hamsters

Received: 28 December 2021

Accepted: 19 January 2022

Accelerated Article Preview Published online 21 January 2022

Cite this article as: Halfmann, P. J. et al. SARS-CoV-2 Omicron virus causes attenuated disease in mice and hamsters. *Nature* https://doi.org/10.1038/s41586-022-04441-6 (2022).

Peter J. Halfmann, Shun Iida, Kiyoko Iwatsuki-Horimoto, Tadashi Maemura, Maki Kiso, Suzanne M. Scheaffer, Tamarand L. Darling, Astha Joshi, Samantha Loeber, Gagandeep Singh, Stephanie L. Foster, Baoling Ying, James Brett Case, Zhenlu Chong, Bradley Whitener, Juan Moliva, Katharine Floyd, Michiko Ujie, Noriko Nakajima, Mutsumi Ito, Ryan Wright, Ryuta Uraki, Prajakta Warang, Matthew Gagne, Rong Li, Yuko Sakai-Tagawa, Yanan Liu, Deanna Larson, Jorge E. Osorio, Juan P. Hernandez-Ortiz, Amy R. Henry, Karl Ciouderis, Kelsey R. Florek, Mit Patel, Abby Odle, Lok-Yin Roy Wong, Allen C. Bateman, Zhongde Wang, Venkata-Viswanadh Edara, Zhenlu Chong, John Franks, Trushar Jeevan, Thomas Fabrizio, Jennifer DeBeauchamp, Lisa Kercher, Patrick Seiler, Ana Silvia Gonzalez-Reiche, Emilia Mia Sordillo, Lauren A. Chang, Harm van Bakel, Viviana Simon, Daniel C. Douek, Nancy J. Sullivan, Larissa B. Thackray, Hiroshi Ueki, Seiya Yamayoshi, Masaki Imai, Stanley Perlman, Richard J. Webby, Robert A. Seder, Mehul S. Suthar, Adolfo García-Sastre, Michael Schotsaert, Tadaki Suzuki, Adrianus C. M. Boon, Michael S. Diamond & Yoshihiro Kawaoka

SARS-CoV-2 Omicron virus causes attenuated disease in mice and hamsters

Peter J. Halfmann[1,26], Shun Iida[2,26], Kiyoko Iwatsuki-Horimoto[3,26], Tadashi Maemura[1,26], Maki Kiso[3,26], Suzanne M. Scheaffer[4], Tamarand L. Darling[4], Astha Joshi[4], Samantha Loeber[5], Gagandeep Singh[6,7], Stephanie L. Foster[8], Baoling Ying[4], James Brett Case[4], Zhenlu Chong[4], Bradley Whitener[4], Juan Moliva[9], Katharine Floyd[8], Michiko Ujie[3], Noriko Nakajima[2], Mutsumi Ito[3], Ryan Wright[1], Ryuta Uraki[3,10], Prajakta Warang[6,7], Matthew Gagne[9], Rong Li[11], Yuko Sakai-Tagawa[3], Yanan Liu[11], Deanna Larson[11], Jorge E. Osorio[12,13], Juan P. Hernandez-Ortiz[13], Amy R. Henry[9], Karl Ciouderis[13], Kelsey R. Florek[14], Mit Patel[8], Abby Odle[15], Lok-Yin Roy Wong[15], Allen C. Bateman[14], Zhongde Wang[11], Venkata-Viswanadh Edara[8], Zhenlu Chong[4], John Franks[16], Trushar Jeevan[16], Thomas Fabrizio[16], Jennifer DeBeauchamp[16], Lisa Kercher[16], Patrick Seiler[16], Ana Silvia Gonzalez-Reiche[17], Emilia Mia Sordillo[18], Lauren A Chang[6,7,19], Harm van Bakel[17], Viviana Simon[6,17,18,20], **Consortium Mount Sinai Pathogen Surveillance (PSP) study group***, Daniel C. Douek[9], Nancy J. Sullivan[9], Larissa B. Thackray[4], Hiroshi Ueki[3,10], Seiya Yamayoshi[3,10], Masaki Imai[3,10], Stanley Perlman[15], Richard J. Webby[16], Robert A. Seder[9], Mehul S. Suthar[8,21], Adolfo García-Sastre[6,7,18,20,22], Michael Schotsaert[6,7], Tadaki Suzuki[2], Adrianus C.M. Boon[4,23,24]†, Michael S. Diamond[4,23,24,25]† & Yoshihiro Kawaoka[1,3,10]†

[1]Influenza Research Institute, Department of Pathobiological Sciences, School of Veterinary Medicine, University of Wisconsin-Madison, Madison, WI, USA.

[2]Department of Pathology, National Institute of Infectious Diseases, Shinjuku-ku, Tokyo, 162-8640 Japan

[3]Division of Virology, Institute of Medical Science, University of Tokyo, Tokyo, Japan

[4]Department of Medicine, Washington University School of Medicine, St. Louis, MO, USA

[5]Department of Surgical Sciences, School of Veterinary Medicine, University of Wisconsin-Madison, WI 53706, USA

[6]Department of Microbiology, Icahn School of Medicine at Mount Sinai New York, NY, USA

[7]Global Health and Emerging Pathogens Institute, Icahn School of Medicine at Mount Sinai New York, NY, USA

[8]Center for Childhood Infections and Vaccines of Children's Healthcare of Atlanta, Department of Pediatrics, Emory Vaccine Center, Emory University School of Medicine, Atlanta, GA, USA.

[9]Vaccine Research Center, National Institute of Allergy and Infectious Diseases, National Institutes of Health, Bethesda, MD USA

[10]The Research Center for Global Viral Diseases, National Center for Global Health and Medicine Research Institute, Tokyo Japan.

[11]Department of Animal Dairy, and Veterinary Sciences, College of Agriculture and Applied Sciences, Utah State University, Logan, UT, USA.

[12]Department of Pathobiological Sciences, School of Veterinary Medicine. University of Wisconsin, Madison, WI, USA.

[13]Colombia/Wisconsin One-Health Consortium and One-Health Genomic Laboratory, Universidad Nacional de Colombia, Medellín, Colombia.

[14]Wisconsin State Laboratory of Hygiene, Madison, WI, USA.

[15]Department of Microbiology and Immunology, University of Iowa, Iowa City, IA, USA.

[16]Department of Infectious Diseases, St. Jude Children's Research Hospital, Memphis, Tennessee, USA

[17]Department of Genetics and Genomic Sciences, Icahn School of Medicine at Mount Sinai New York, NY, USA

[18]Department of Pathology, Molecular and Cell-Based Medicine, Icahn School of Medicine at Mount Sinai New York, NY, USA

[19]Graduate School of Biomedical Sciences, Icahn School of Medicine at Mount Sinai, New York, NY, USA.

[20]Department of Medicine, Division of Infectious Diseases, Icahn School of Medicine at Mount Sinai New York, NY, USA

[21]Department of Microbiology and Immunology, Emory University, Atlanta, GA, USA

[22]The Tisch Cancer Institute, Icahn School of Medicine at Mount Sinai New York, NY, USA

[23]Department of Pathology & Immunology, Washington University School of Medicine, St. Louis, MO, USA.

[24]Department of Molecular Microbiology, Washington University School of Medicine, St. Louis, MO, USA

[25]The Andrew M. and Jane M. Bursky Center for Human Immunology and Immunotherapy Programs, Washington University School of Medicine. St. Louis, MO USA

[26]These authors contributed equally: Peter J. Halfmann, Shun Iida, Kiyoko Iwatsuki-Horimoto, Tadashi Maemura, Maki Kiso

*A list of authors and their affiliations appears at the end of the paper.

†e-mail: yoshihiro.kawaoka@wisc.edu; mdiamond@wustl.edu; jboon@wustl.edu

The recent emergence of B.1.1.529, the Omicron variant[1,2] has raised concerns for escape from protection by vaccines and therapeutic antibodies. A key test for potential countermeasures against B.1.1.529 is their activity in pre-clinical rodent models of respiratory tract disease. Here, using the collaborative network of the SARS-CoV-2 Assessment of Viral Evolution (SAVE) program of the National Institute of Allergy and Infectious Diseases (NIAID), we evaluated the ability of multiple B.1.1.529 Omicron isolates to cause infection and disease in immunocompetent and human ACE2 (hACE2) expressing mice and hamsters. Despite modeling data suggesting that B.1.1.529 spike can bind more avidly to murine ACE2[3,4], we observed less infection in 129, C57BL/6, BALB/c, and K18-hACE2 transgenic mice as compared with previous SARS-CoV-2 variants, with limited weight loss and lower viral burden in the upper and lower respiratory tracts. In wild-type and hACE2 transgenic hamsters, lung infection, clinical disease, and pathology with B.1.1.529 also were milder compared to historical isolates or other SARS-CoV-2 variants of concern. Overall, experiments from the SAVE/NIAID network with several B.1.1.529 isolates demonstrate attenuated lung disease in rodents, which parallels preliminary human clinical data.

Severe acute respiratory syndrome coronavirus 2 (SARS-CoV-2) has caused a pandemic resulting in millions of deaths worldwide**.** The extensive morbidity and mortality made the development of vaccines, antibody-based countermeasures, and antiviral agents a global health priority. As part of this process, several models of SARS-CoV-2 infection and lung pathogenesis were developed in animals for rapid testing[5]. Remarkably, several highly effective vaccines and therapeutics were deployed with billions of doses given worldwide. While these measures

markedly reduced hospitalizations and deaths, their efficacy has been jeopardized by emergence of SARS-CoV-2 variants with mutations in the spike gene.

The SARS-CoV-2 spike protein engages angiotensin-converting enzyme 2 (ACE2) on the surface of human cells to facilitate entry and infection of cells[6]. Upon cell attachment, spike proteins are cleaved by host proteases into S1 and S2 fragments. The S1 protein includes the N-terminal and receptor binding (RBD) domains. The RBD is the target of many potently neutralizing monoclonal[7-11] and serum polyclonal antibodies[12]. Although SARS-CoV-2 spike proteins from strains early in the pandemic bound to ACE2 from multiple animal species (*e.g.*, hamster, ferret, and nonhuman primates), they did not bind mouse ACE2, which explained why laboratory strains of mice could not be infected by SARS-CoV-2[6,13]; indeed, mice could become susceptible through expression of hACE2 via a transgene[14-16], viral vector[17,18], or under regulation of the mouse ACE2 promoter[19-21]. Later in the pandemic, several strains acquired a mouse-adapting spike substitution (N501Y), which allowed engagement of murine ACE2 and productive infection of mice without hACE2 expression[22-24].

In late November of 2021, the Omicron (B.1.1.529) variant emerged, which has the largest number (>30) of substitutions, deletions, or insertions in the spike protein described to date. This has raised concerns for escape from protection by vaccines and therapeutic mAbs. B.1.1.529 isolates have many changes in the RBD (G339D, R346K, S371L, S373P, S375F, K417N, N440K, G446S, S477N, T478K, E484A, Q493R, G496S, Q498R, N501Y, and Y505H). The N501Y substitution along with changes at sites (K417, E484, Q493, Q498, and N501) associated with mouse adaptation[25-30] suggested that B.1.1.529 should infect mice[3]. One study speculated that the progenitor of B.1.1.529 jumped from humans to mice, and then back into humans[4]. In support of this, B.1.1.529 RBD binds to murine ACE2[31]. Lastly, hamsters have been

a valuable animal model for assessing countermeasures against SARS-CoV-2 and variants. Hamsters are susceptible to SARS-CoV-2 infection with similar pathological changes seen in lung tissues from COVID-19 patients[5,32,33]. Here, using data from multiple laboratories of the SAVE/NIAID consortium (**Supplementary Table 1**), we report on the infectivity of multiple B.1.1.529 isolates in mice and hamsters, two key rodent models of SARS-CoV-2 infection and pathogenesis.

B.1.1.529 infection in mice

Based on the presence of several mutations that are considered mouse-adapting, we predicted that B.1.1.529 should infect immunocompetent mice and cause lung disease as seen with other recombinant strains (WA1/2020 N501Y) or variants (*e.g.*, B.1.351) containing N501Y substitutions. We first tested B.1.1.529 in 129 mice. Two laboratories (M.S. [Atlanta] and A.G.S. [New York]) independently inoculated 6 to 8-week-old (A.G.S.) or 10 to 20-week-old (M.S.) 129 mice with 10^4, 10^5 or 10^6 infectious units (plaque- [PFU] or focus-forming [FFU] units) of three different B.1.1.529 strains (**Supplementary Tables 1-2**). Since 129 mice sustain 10 to 15% loss of body weight 3 to 4 days-post-infection (dpi) yet recover and gain weight beginning at 5 dpi[22,34] with SARS-CoV-2 strains encoding N501Y substitutions[34], we assessed weight change with B.1.1.529 at 3 and 4 dpi. However, after inoculation of B.1.1.529, 129 mice failed to lose weight (**Fig 1a**). Similarly, aged (10 to 14-month-old) C57BL/6 mice [S.P.] also did not lose weight after B.1.1.529 infection, whereas those infected with B.1.351 did (**Fig 1a**).

We next compared viral burden in B.1.1.529- and B.1.351-infected 129 mice. At 3 dpi, 129 mice infected with B.1.351 sustained high levels of infection in the nasal wash, nasal turbinates, and lungs (**Fig 1b)**. The levels of viral RNA in the nasal turbinates and lungs of B.1.1.529-infected mice were 10 to 100-fold lower than in B.1.351-infected animals (**Fig 1b**).

Similar results were seen in a separate cohort of 129 mice at 4 dpi, with 1,000 to 100,000-fold less infectious virus recovered from nasal turbinates and lungs of animals infected with B.1.1.529 compared to B.1.351 (**Fig 1c**).

Members of the group (Y.K.) also tested B.1.1.529 in BALB/c mice. At 2 dpi, infectious virus levels in the nasal turbinates and lungs were significantly lower (~1,000-fold, $P < 0.001$) in BALB/c mice infected with B.1.1.529 compared to B.1.351 (**Fig 1d**). We used whole-body plethysmography[35] to measure pulmonary function in infected mice. At 2 dpi, whereas B.1.351 caused an increase ($P < 0.001$) in the lung enhanced pause (Penh), a marker of bronchoconstriction, B.1.1.529 did not (**Fig 1e**). The ratio of peak expiratory flow (Rpef) also was decreased at 2 dpi in BALB/c mice infected with B.1.351 but not B.1.1.529 ($P < 0.001$, **Fig 1e**).

Two groups (M.D. and A.G.S.) tested B.1.1.529 infection in K18-hACE2 transgenic mice, which express hACE2 under an epithelial cytokeratin promoter[14], and are more susceptible to SARS-CoV-2 infection[16]. At intranasal doses ranging from 10^3 to 10^5 infectious units of B.1.1.529, weight loss was not observed over the first 5 to 6 days of infection in younger or older K18-hACE2 mice (**Fig 1f**). These data contrasts with historical results with WA1/2020 D614G or variant (*e.g.*, B.1.351) SARS-CoV-2 strains[16,24,34,36], which uniformly induce weight loss starting at 4 dpi. The groups separately observed reduced levels of infectious B.1.1.529 compared to WA1/2020 D614G or B.1.351 in the lower respiratory tracts at 3 dpi (**Fig 1g-h**). Finally, we assessed inflammatory responses in the lungs of K18-hACE2 mice at 3 dpi. Mice inoculated with B.1.1.529 had lower levels of several pro-inflammatory cytokines and chemokines compared to those inoculated with B.1.351, with many values similar to uninfected controls (**Fig 1i and Supplementary Table 3**). Thus, based on multiple parameters (weight

change, viral burden, respiratory function measurements, and cytokine responses), B.1.1.529 appears attenuated in the respiratory tract of multiple strains of mice.

B.1.1.529 infection in hamsters

Four members of our group (R.S., A.B., R.W., and Y.K.) tested three different B.1.1.529 strains for their ability to infect and cause disease (**Supplementary Table 1**). Whereas intranasal infection with historical or other variant SARS-CoV-2 strains generally resulted in ~10 to 15% reduction in body weight over the first week, we observed no weight loss in hamsters inoculated with B.1.1.529 (**Fig 2a-d**), although animals did not gain body weight as rapidly as uninfected hamsters. Viral RNA analysis at 4 dpi showed lower levels of B.1.1.529 infection in the lungs (12-fold, $P < 0.001$) compared to WA1/2020 D614G ([A.B.]; **Fig 2e**). A comparison of infectious viral burden in tissues at 3 dpi between B.1.617.2 and B.1.1.529 strains [Y.K.] showed virtually no difference in nasal turbinates but substantially less infection of B.1.1.529 in the lungs of most animals (**Fig 2f**). A comparison of viral RNA levels between WA1/2020 and B.1.1.529 (R.W) in nasal washes at 4 dpi did not show substantial differences in titers (**Fig 2g**). Thus, in hamsters, upper, but not lower, respiratory tract infection by B.1.1.529 appears relatively intact.

We used whole-body plethysmography to measure pulmonary function in infected Syrian hamsters (Y.K.). Starting at 3 dpi and continuing until 7 dpi, infection with B.1.617.2 caused an increase ($P < 0.05$) in the lung enhanced pause (Penh), whereas B.1.1.529 infection did not (**Fig 2h,** *left*). The ratio of peak expiratory flow (Rpef) was decreased at 5 and 7 dpi in animals infected with B.1.617.2 but not B.1.1.529 ($P < 0.001$, **Fig 2h,** *middle*). Finally, hamsters infected with B.1.617.2, but not B.1.1.529, demonstrated a decrease in respiratory rate (Frequency)

compared to uninfected animals (**Fig 2h**, *right*). Based on multiple functional parameters, lung infection and disease after B.1.1.529 infection was attenuated compared to other variant strains.

We performed microcomputed tomography (micro-CT) to assess for lung abnormalities in hamsters at 7 dpi. Micro-CT analysis revealed lung abnormalities in all B.1.617.2-infected hamsters on 7 dpi that were consistent with commonly reported imaging features of COVID-19 pneumonia[37]. In comparison, analysis of B.1.1.529-infected hamsters on 7 dpi revealed patchy, ill-defined ground glass opacity consistent with minimal to mild pneumonia. Syrian hamsters infected with B.1.617.2 had a much higher CT disease score[35] than those infected with B.1.1.529 (**Fig 2i-j**).

Members of our group [T.S.] also compared lung pathology in Syrian hamsters after infection with B.1.617.2 or B.1.1.529. The lungs obtained from B.1.617.2-infected hamsters showed congestion and/or hemorrhage, which was absent in B.1.1.529-infected animals (**Fig. 3a**). Immune cell infiltration and inflammation were present in the peribronchial regions of the lungs at 3 dpi with B.1.617.2. At 6 dpi, extensive infiltration of neutrophils and lymphocytes in the alveolar space was accompanied by pulmonary edema and hemorrhage (**Fig 3b**, *inset*), and regenerative changes in the bronchial epithelia became prominent (**Fig 3b**). In contrast, in B.1.1.529-infected hamsters, small foci of inflammation in the alveoli and peribronchial regions were observed only at 6 dpi (**Fig 3b**). A worse histopathology score of viral pneumonia at 6 dpi was measured after B.1.617.2 than B.1.1.529 infection (**Fig 3c**). After B.1.617.2 infection, viral RNA was detected readily in the alveoli and bronchial epithelia at 3 and 6 dpi (**Fig 3d**). After B.1.1.529 infection, fewer bronchial epithelial cells and alveoli were positive for viral RNA at either time point (**Fig 3d**). Thus, B.1.1.529 replicates less efficiently in the lungs of Syrian hamsters, which results in less severe pneumonia compared to the B.1.617.2 variant.

Even though hamster ACE2 can serve as a receptor for SARS-CoV-2 spike protein, some of the contact residues in hACE2 are not conserved[38], which could diminish infectivity. To develop a more susceptible hamster model, members of the consortium (Y.K.) used transgenic hamsters (generated by Z.W.) expressing hACE2 under the epithelial cytokeratin-18 promoter[39]. Whereas intranasal inoculation of 10^3 PFU of HP-095 D614G virus resulted in marked weight loss within the first week (**Fig 2k**) and uniform mortality by 10 dpi (**Fig 2l**), less weight loss and death ($P < 0.05$) were observed after infection with B.1.1.529. Moreover, 1,000 to 10,000-fold lower levels of infectious virus were measured in the lungs of hACE2 transgenic hamsters challenged with B.1.1.529 than HP-095 D614G at 3 and 5 dpi (**Fig 2m**). As seen in wild-type Syrian hamsters, smaller differences in infection were observed in the nasal turbinates. Thus, B.1.1.529 infection in the lung is attenuated in both wild-type and hACE2 transgenic hamsters.

Discussion

Our experiments suggest that the B.1.1.529 Omicron variant is attenuated in laboratory mice and hamsters. While these results are consistent with preliminary data in humans[40,41], the basis for attenuation remains unknown. One study suggests that B.1.1.529 replicates faster in the human bronchus and less in lung cells, which may explain its greater transmissibility and putative lower disease severity[42]. We observed less B.1.1.529 infection of hamster bronchial cells *in vivo* and lower viral burden in nasal washes and turbinates in mice compared to other SARS-CoV-2 strains. The attenuation in mice was unexpected given that B.1.1.529 has mutations in the RBD that are sites associated with adaptation for mice[25-27]. The attenuation in hamsters seen by our group and others[43] also was surprising, given that other SARS-CoV-2 variants replicate to high levels in this animal[35,44,45]. Whereas the more than 30 changes in the B.1.1.529 spike protein could impact receptor engagement, changes in other proteins could affect replication,

temperature sensitivity, cell and tissue tropism, and induction of pro-inflammatory responses in a species-specific manner. Our results showing attenuated B.1.1.529 infection in laboratory mice do not support the suggestion that B.1.1.529 has a mouse origin[4]. However, infection studies in wild mice[46] are needed to fully address this question.

Although B.1.1.529 is less pathogenic in mice and hamsters, these animals still will have utility in evaluating vaccine, antibody, or small molecule inhibitors. The mice and hamsters tested, to varying degrees, showed evidence of viral replication and dissemination to the lower respiratory tract, which could be mitigated by countermeasures. The most severe B.1.1.529 infection and disease was observed in hACE2 expressing mice and hamsters, which is consistent with other SARS-CoV-2 strains[16,24,39,47], and possibly related to the enhanced interactions between hACE2 and the B.1.1.529 spike[48]. Indeed, structural analysis of the B.1.1.529 spike protein in complex with hACE2 reveals new interactions formed by mutated residues in the RBD[48,49].

These *in vivo* studies were performed as part of the SAVE/NIAID consortium and reflect a network that communicates weekly to expedite progress on SARS-CoV-2 variants. This format had several advantages: (a) Animal experiments were reproduced across laboratories providing confidence in results; (b) Multiple B.1.1.529 isolates were tested limiting the possibility of sequence adaptations in a strain from one laboratory that could skew results; (c) Multiple strains of mice and hamsters at different ages were tested allowing for a comprehensive data set; and (d) The groups used overlapping metrics to evaluate infection and disease in the different animal models.

We note several limitations to our study: (1) Our experiments reflect data from a consortium that did not use uniform study design and metrics, which created variability in

outcomes; despite this, data from multiple groups suggest B.1.1.529 is attenuated in rodent models; (2) While attenuation of B.1.1.529 in mice and hamsters correlates with preliminary data in humans, evaluation in NHPs and unvaccinated, previously uninfected humans are needed for corroboration. (3) We used the prevailing B.1.1.529 Omicron isolate that lacks an R346K substitution. While ~10% of B.1.1.529 sequences in GISAID currently have an R346K sequence, this substitution or others in genes apart from spike might affect virulence. Although one of the B.1.1.529 isolates we tested contains an additional A701V change in spike near the furin cleavage site, it was still attenuated in mice; (4) Detailed pathological and immunological analyses were not performed for all of the animal species studied. It remains possible that B.1.1.529 is attenuated clinically (*e.g.*, weight loss) because of defects in promoting pathological host responses.

In summary, our collective studies rapidly and reproducibly demonstrated attenuated infection in multiple strains of mice and hamsters. Experiments are ongoing to determine the basis for attenuation in mice and hamsters and to determine how this relates to B.1.1.529 Omicron infection in humans.

Online content Any methods, additional references, Nature Research reporting summaries, source data, extended data, supplementary information, acknowledgements, peer review information; details of author contributions and competing interests; and statements of data and code availability are available at

Received 28 December 2021; accepted 19 January 2022

1 Callaway, E. & Ledford, H. How bad is Omicron? What scientists know so far. *Nature*, doi:10.1038/d41586-021-03614-z (2021).

2 Torjesen, I. Covid-19: Omicron may be more transmissible than other variants and partly resistant to existing vaccines, scientists fear. *BMJ (Clinical research ed* **375**, n2943, doi:10.1136/bmj.n2943 (2021).

3 Kuiper, M. J. *et al.* But Mouse, you are not alone: On some severe acute respiratory syndrome coronavirus 2 variants infecting mice. *bioRxiv*, 2021.2008.2004.455042, doi:10.1101/2021.08.04.455042 (2021).

4 Wei, C. *et al.* Evidence for a mouse origin of the SARS-CoV-2 Omicron variant. *bioRxiv*, 2021.2012.2014.472632, doi:10.1101/2021.12.14.472632 (2021).
5 Muñoz-Fontela, C. *et al.* Animal models for COVID-19. *Nature* **586**, 509-515, doi:10.1038/s41586-020-2787-6 (2020).
6 Letko, M., Marzi, A. & Munster, V. Functional assessment of cell entry and receptor usage for SARS-CoV-2 and other lineage B betacoronaviruses. *Nature microbiology* **5**, 562-569, doi:10.1038/s41564-020-0688-y (2020).
7 Pinto, D. *et al.* Cross-neutralization of SARS-CoV-2 by a human monoclonal SARS-CoV antibody. *Nature* **583**, 290-295, doi:10.1038/s41586-020-2349-y (2020).
8 Cao, Y. *et al.* Potent neutralizing antibodies against SARS-CoV-2 identified by high-throughput single-cell sequencing of convalescent patients' B cells. *Cell* **182**, 73-84, doi:10.1016/j.cell.2020.05.025 (2020).
9 Zost, S. J. *et al.* Rapid isolation and profiling of a diverse panel of human monoclonal antibodies targeting the SARS-CoV-2 spike protein. *Nat Med* **26**, 1422-1427, doi:10.1038/s41591-020-0998-x (2020).
10 Barnes, C. O. *et al.* SARS-CoV-2 neutralizing antibody structures inform therapeutic strategies. *Nature* **588**, 682-687, doi:10.1038/s41586-020-2852-1 (2020).
11 Tortorici, M. A. *et al.* Ultrapotent human antibodies protect against SARS-CoV-2 challenge via multiple mechanisms. *Science* **370**, 950-957, doi:10.1126/science.abe3354 (2020).
12 Rathe, J. A. *et al.* SARS-CoV-2 Serologic Assays in Control and Unknown Populations Demonstrate the Necessity of Virus Neutralization Testing. *J Infect Dis*, doi:10.1093/infdis/jiaa797 (2020).
13 Wan, Y., Shang, J., Graham, R., Baric, R. S. & Li, F. Receptor recognition by novel coronavirus from Wuhan: An analysis based on decade-long structural studies of SARS. *J Virol*, doi:10.1128/jvi.00127-20 (2020).
14 McCray, P. B., Jr. *et al.* Lethal infection of K18-hACE2 mice infected with severe acute respiratory syndrome coronavirus. *J Virol* **81**, 813-821, doi:10.1128/jvi.02012-06 (2007).
15 Jiang, R. D. *et al.* Pathogenesis of SARS-CoV-2 in Transgenic Mice Expressing Human Angiotensin-Converting Enzyme 2. *Cell*, doi:10.1016/j.cell.2020.05.027 (2020).
16 Winkler, E. S. *et al.* SARS-CoV-2 infection of human ACE2-transgenic mice causes severe lung inflammation and impaired function. *Nat Immunol* **21**, 1327-1335, doi:10.1038/s41590-020-0778-2 (2020).
17 Hassan, A. O. *et al.* A SARS-CoV-2 Infection Model in Mice Demonstrates Protection by Neutralizing Antibodies. *Cell*, doi:10.1016/j.cell.2020.06.011 (2020).
18 Sun, J. *et al.* Generation of a Broadly Useful Model for COVID-19 Pathogenesis, Vaccination, and Treatment. *Cell* **182**, 734-743.e735, doi:10.1016/j.cell.2020.06.010 (2020).
19 Bao, L. *et al.* The pathogenicity of SARS-CoV-2 in hACE2 transgenic mice. *Nature*, doi:10.1038/s41586-020-2312-y (2020).
20 Sun, S. H. *et al.* A Mouse Model of SARS-CoV-2 Infection and Pathogenesis. *Cell Host Microbe*, doi:10.1016/j.chom.2020.05.020 (2020).
21 Winkler, E. S. *et al.* SARS-CoV-2 causes lung infection without severe disease in human ACE2 knock-in mice. *J Virol*, Jvi0151121, doi:10.1128/jvi.01511-21 (2021).
22 Rathnasinghe, R. *et al.* The N501Y mutation in SARS-CoV-2 spike leads to morbidity in obese and aged mice and is neutralized by convalescent and post-vaccination human sera.

medRxiv : the preprint server for health sciences, doi:10.1101/2021.01.19.21249592 (2021).

23 Gu, H. *et al.* Adaptation of SARS-CoV-2 in BALB/c mice for testing vaccine efficacy. *Science* **369**, 1603-1607, doi:10.1126/science.abc4730 (2020).

24 Chen, R. E. *et al.* In vivo monoclonal antibody efficacy against SARS-CoV-2 variant strains. *Nature*, doi:10.1038/s41586-021-03720-y (2021).

25 Kibler, K. V. *et al.* Intranasal immunization with a vaccinia virus vaccine vector expressing pre-fusion stabilized SARS-CoV-2 spike fully protected mice against lethal challenge with the heavily mutated mouse-adapted SARS2-N501Y_{MA30} strain of SARS-CoV-2. *bioRxiv*, 2021.2012.2006.471483, doi:10.1101/2021.12.06.471483 (2021).

26 Leist, S. R. *et al.* A Mouse-Adapted SARS-CoV-2 Induces Acute Lung Injury and Mortality in Standard Laboratory Mice. *Cell* **183**, 1070-1085.e1012, doi:10.1016/j.cell.2020.09.050 (2020).

27 Dinnon, K. H., 3rd *et al.* A mouse-adapted model of SARS-CoV-2 to test COVID-19 countermeasures. *Nature* **586**, 560-566, doi:10.1038/s41586-020-2708-8 (2020).

28 Roy Wong, L.-Y. *et al.* Eicosanoid signaling as a therapeutic target in middle-aged mice with severe COVID-19. *bioRxiv*, 2021.2004.2020.440676, doi:10.1101/2021.04.20.440676 (2021).

29 Vanderheiden, A. *et al.* CCR2 Signaling Restricts SARS-CoV-2 Infection. *mBio* **12**, e0274921, doi:10.1128/mBio.02749-21 (2021).

30 Muruato, A. *et al.* Mouse-adapted SARS-CoV-2 protects animals from lethal SARS-CoV challenge. *PLoS Biol* **19**, e3001284, doi:10.1371/journal.pbio.3001284 (2021).

31 Cameroni, E. *et al.* Broadly neutralizing antibodies overcome SARS-CoV-2 Omicron antigenic shift. *bioRxiv*, 2021.2012.2012.472269, doi:10.1101/2021.12.12.472269 (2021).

32 Sia, S. F. *et al.* Pathogenesis and transmission of SARS-CoV-2 in golden hamsters. *Nature* **583**, 834-838, doi:10.1038/s41586-020-2342-5 (2020).

33 Imai, M. *et al.* Syrian hamsters as a small animal model for SARS-CoV-2 infection and countermeasure development. *Proc Natl Acad Sci U S A* **117**, 16587-16595, doi:10.1073/pnas.2009799117 (2020).

34 Ying, B. *et al.* Protective activity of mRNA vaccines against ancestral and variant SARS-CoV-2 strains. *Sci Transl Med*, eabm3302 (2021).

35 Imai, M. *et al.* Characterization of a new SARS-CoV-2 variant that emerged in Brazil. *Proc Natl Acad Sci U S A* **118**, doi:10.1073/pnas.2106535118 (2021).

36 Winkler, E. S. *et al.* Human neutralizing antibodies against SARS-CoV-2 require intact Fc effector functions for optimal therapeutic protection. *Cell* **184**, 1804-1820.e1816, doi:10.1016/j.cell.2021.02.026 (2021).

37 Simpson, S. *et al.* Radiological Society of North America Expert Consensus Statement on Reporting Chest CT Findings Related to COVID-19. Endorsed by the Society of Thoracic Radiology, the American College of Radiology, and RSNA - Secondary Publication. *Journal of thoracic imaging* **35**, 219-227, doi:10.1097/rti.0000000000000524 (2020).

38 Damas, J. *et al.* Broad host range of SARS-CoV-2 predicted by comparative and structural analysis of ACE2 in vertebrates. *Proc Natl Acad Sci U S A* **117**, 22311-22322, doi:10.1073/pnas.2010146117 (2020).

39 Gilliland, T. *et al.* Protection of human ACE2 transgenic Syrian hamsters from SARS CoV-2 variants by human polyclonal IgG from hyper-immunized transchromosomic bovines. *bioRxiv*, doi:10.1101/2021.07.26.453840 (2021).
40 Espenhain, L. *et al.* Epidemiological characterisation of the first 785 SARS-CoV-2 Omicron variant cases in Denmark, December 2021. *Euro Surveill* **26**, doi:10.2807/1560-7917.es.2021.26.50.2101146 (2021).
41 Kupferschmidt, K. & Vogel, G. How bad is Omicron? Some clues are emerging. *Science* **374**, 1304-1305, doi:10.1126/science.acx9782 (2021).
42 Michael, C. W. C. *et al. Nature Portfolio*, doi:10.21203/rs.3.rs-1189219/v1 (2021).
43 Abdelnabi, R. *et al.* The omicron (B.1.1.529) SARS-CoV-2 variant of concern does not readily infect Syrian hamsters. *bioRxiv*, 2021.2012.2024.474086, doi:10.1101/2021.12.24.474086 (2021).
44 Yadav, P. *et al.* Isolation of SARS-CoV-2 B.1.1.28.2 (P2) variant and pathogenicity comparison with D614G variant in hamster model. *Journal of infection and public health* **15**, 164-171, doi:10.1016/j.jiph.2021.12.009 (2021).
45 Ulrich, L. *et al.* Enhanced fitness of SARS-CoV-2 variant of concern Alpha but not Beta. *Nature*, doi:10.1038/s41586-021-04342-0 (2021).
46 Griffin, B. D. *et al.* SARS-CoV-2 infection and transmission in the North American deer mouse. *Nat Commun* **12**, 3612, doi:10.1038/s41467-021-23848-9 (2021).
47 Zheng, J. *et al.* COVID-19 treatments and pathogenesis including anosmia in K18-hACE2 mice. *Nature* **589**, 603-607, doi:10.1038/s41586-020-2943-z (2021).
48 Mannar, D. *et al.* SARS-CoV-2 Omicron Variant: ACE2 Binding, Cryo-EM Structure of Spike Protein-ACE2 Complex and Antibody Evasion. *bioRxiv*, 2021.2012.2019.473380, doi:10.1101/2021.12.19.473380 (2021).
49 McCallum, M. *et al.* Structural basis of SARS-CoV-2 Omicron immune evasion and receptor engagement. *bioRxiv*, 2021.2012.2028.474380, doi:10.1101/2021.12.28.474380 (2021).

Consortium Mount Sinai Pathogen Surveillance (PSP) study group

B. Alburquerque[17], H. Alshammary[6], A. A. Amoako[6], S. Aslam[6], R. Banu[18], C. Cognigni[6], M. Espinoza-Moraga[6], K. Farrugia[17], A. van de Guchte[17], Z. Khalil[17], M. Laporte[6], I. Mena[6], A. E. Paniz-Mondolfi[18], J. Polanco[18], A. Rooker[6], L. A. Sominsky[6]

METHODS

Cells

Vero-TMPRSS2[35,50,51] and Vero-hACE2-TMPRSS2[52] cells were cultured at 37°C in Dulbecco's Modified Eagle medium (DMEM) supplemented with 10% fetal bovine serum (FBS), 10 mM HEPES pH 7.3, and 100 U/mL of penicillin–streptomycin. Vero-TMPRSS2 cells were supplemented with 5 μg/mL of blasticidin or 1 mg/mL of geneticin (depending on the cell line) and in some cultures with plasmocin. Vero-hACE2-TMPRSS2 cells were supplemented with 10 μg/mL of puromycin. All cells routinely tested negative for mycoplasma using a PCR-based assay.

Viruses

The WA1/2020 recombinant strains with substitutions (D614G and/or N501Y/D614G) were described previously[53]. The B.1.1.529 isolates (hCoV-19/USA/WI-WSLH-221686/2021 [Y.K., M.S.D., R.A.S., A.C.M.B., GISAID: EPI_ISL_7263803], hCoV-19/Japan/NC928-2N/2021 (NC928) [Y.K., GISAID: EPI_ISL_7507055], hCoV-19/USA/NY-MSHSPSP-PV44476/2021 [A.G.S. and Mount Sinai Pathogen Surveillance Program, GISAID: EPI_ISL_7908052], hCoV-19/USA/NY-MSHSPSP-PV44488/2021 [A.G.S. and Mount Sinai Pathogen Surveillance Program, GISAID: EPI_ISL_7908059], and hCoV-19/USA/GA-EHC-2811C/2021 [M.S.S., S.P., and R.J.W. GISAID: EPI_ISL_7171744]) were obtained from nasal swabs and passaged on Vero-TMPRSS2 cells as described[33,35,51]. Sequence differences between B.1.1.529 isolates are depicted in **Supplemental Table 2**. Other viruses used included: SARS-CoV-2/UT-HP095-1N/Human/2020/Tokyo (HP-095; D614G), hCoV-19/USA/CA_CDC_5574/2020 (Alpha, B.1.1.7; BEI NR54011), hCoV-19/USA/MD-HP01542/2021 (Beta, B.1.351), 20H/501Y.V2 (Beta, B.1.351), hCoV-19/USA/PHC658/202 (Delta, B.1.617.2), and hCoV-19/USA/WI-UW-

5250/2021 (Delta, B.1.617.2; UW-5250)[54]. All viruses were subjected to next-generation sequencing as described[55] to confirm the stability of substitutions and avoid introduction of adventitious mutations. All virus experiments were performed in an approved biosafety level 3 (BSL-3) facility.

Animal experiments and approvals

Animal studies were carried out in accordance with the recommendations in the Guide for the Care and Use of Laboratory Animals of the National Institutes of Health. The protocols were approved by the Institutional Animal Care and Use Committee at the Washington University School of Medicine (assurance number A3381–01), University of Wisconsin, Madison (V006426), St. Jude Children's Research Hospital (Assurance number D16-00043), Emory University, University of Iowa (assurance number A3021-01), Icahn School of Medicine at Mount Sinai (PROTO202100007), BIOQUAL, Inc., and the Animal Experiment Committee of the Institute of Medical Science, the University of Tokyo (approval numbers PA19-72 and PA19-75). Virus inoculations were performed under anesthesia that was induced and maintained with ketamine hydrochloride and xylazine, and all efforts were made to minimize animal suffering. *In vivo* studies were not blinded, and animals were randomly assigned to infection groups. No sample-size calculations were performed to power each study. Instead, sample sizes were determined based on prior *in vivo* virus challenge experiments.

Mouse infection experiments

Heterozygous K18-hACE2 C57BL/6J mice (strain 2B6.Cg-Tg(K18-ACE2)2Prlmn/J), 129 mice (strain: 129S2/SvPasCrl or 129S1/SvImJ), and C57BL/6 (strain 000664) mice were obtained from The Jackson Laboratory and Charles River Laboratories. BALB/c mice were purchased from Japan SLC Inc. Animals were housed in groups and fed standard chow diets.

Infection experiments were performed as follows: (a) [M.S.D] 5-month-old female K18-hACE2 mice were inoculated by intranasal route with 10^3, 10^4 or 10^5 FFU of SARS-CoV-2. (b) [M.S.S.] 129S1 male and female mice were used were between 10-20 weeks of age. Mice were anesthetized with isoflurane and inoculated intranasally with virus (50 μL, 10^6 PFU/mouse); (c) [Y.K.] Six-week-old female BALB/c mice were inoculated intranasally with 10^5 PFU of hCoV-19/Japan/NC928-2N/2021 or hCoV-19/USA/MD-HP01542/2021; (d) [S.P.] Retired breeder female C57BL/6 mice (10 to 14-month-old) were anesthetized with ketamine-xylazine and inoculated intranasally with SARS-CoV-2 in a total volume of 50 μL of DMEM. Animal weight and health were monitored daily; and (e) [A.G.S.] 6-8-week-old female 129S1 mice and 6-month-old female K18-hACE2 mice were inoculated by intranasal route under light ketamine/xylazine sedation with 10^4 PFU of hCoV-19/USA/NY-MSHSPSP-PV44476/2021 or hCoV-19/USA/NY-MSHSPSP-PV44488/2021 in a total volume of 50 μL.

Hamster infection experiments

Five-to-six-week-old male Syrian Golden hamsters were obtained from Charles River Laboratories, Envigo, or Japan SLC Inc. The K18-hACE2 transgenic hamster line was developed with a piggyBac-mediated transgenic approach, in which the K18-hACE2 cassette from the pK18-hACE2 plasmid[14] was transferred into a piggyBac vector, pmhyGENIE-3[56], for pronuclear injection. hACE2 transgenic hamsters will be described in detail elsewhere[39]. Twelve-month-old transgenic female animals were used. Infection experiments were performed as follows: (a) [A.C.M.B] animals were challenged via intranasal route with 10^3 PFU of WA1/2020 D614G or B.1.1.529 variant in 100 μL; (b) [Y.K.] Under isoflurane anesthesia, wild-type Syrian hamsters were intranasally inoculated with 10^3 PFU of SARS-CoV-2 strains in 30 μL. Body weight was monitored daily. For virological and pathological examinations, four hamsters per group were

euthanized 3 and 6 dpi, and nasal turbinates and lungs were collected. The virus titers in the nasal turbinates and lungs were determined by plaque assays on Vero-TMPRSS2 cells. Human ACE2 transgenic hamsters were intranasally inoculated with 10^3 PFU of HP-095 D614G or B.1.1.529 [hCoV-19/USA/WI-WSLH-221686/2021] in 50 µL. Body weight and survival were monitored daily, and nasal turbinates and lungs were collected at 3 and 5 dpi for virological analysis; (c) [R.A.S.] Six-week-old male Syrian golden hamsters were randomized into groups of 4 to 6 and inoculated with SARS-CoV-2 via delivery of 100 µL of appropriately diluted virus in PBS equally split between both nostrils. Weight change and clinical observations were collected daily; and (d) [R.J.W] while under isoflurane anesthesia, male 8-10 week old hamsters were inoculated intranasally with 10^4 PFU of WA1/2020 or B.1.1.529 in 100 µL volume. Body weight and survival were monitored daily. Nasal washes were taken at 4 dpi for virological analysis.

Measurement of viral burden

(a) Mouse studies.

[M.S.D.] Tissues were weighed and homogenized with zirconia beads in a MagNA Lyser instrument (Roche Life Science) in 1000 µL of DMEM medium supplemented with 2% heat-inactivated FBS. Tissue homogenates were clarified by centrifugation at 10,000 rpm for 5 min and stored at −80°C. RNA was extracted using the MagMax mirVana Total RNA isolation kit (Thermo Fisher Scientific) on the Kingfisher Flex extraction robot (Thermo Fisher Scientific). Viral RNA (*N* gene) was reverse transcribed and amplified using the TaqMan RNA-to-CT 1-Step Kit (Thermo Fisher Scientific), and data were analyzed and normalized as described previously[57]. Infectious virus titers were determined by plaque assay on Vero-hACE2-TMPRSS2 cells as previously published[24]. [Y.K.] The viral titers in the nasal turbinates and lungs were determined by plaque assay on Vero-TMPRSS2 cells as previously published[51]. [M.S.S.] At the

indicated day post-infection, mice were euthanized with isoflurane overdose and one lobe of lung tissue was collected in an Omni Bead ruptor tube filled with Tri Reagent (Zymo, #R2050-1-200). Tissue was homogenized using an Omni Bead Ruptor 24 (5.15 ms, 15 seconds), then centrifuged to remove debris. RNA was extracted using a Direct-zol RNA MiniPrep Kit (Zymo, # R2051), then converted to cDNA using a High-capacity Reverse Transcriptase cDNA Kit (Thermo, #4368813). SARS-CoV-2 RNA-dependent RNA polymerase and subgenomic RNA were measured as described[29,58]. [M.S.S.] The subgenomic SARS-CoV-2 RNA levels were quantified in nasal turbinates and lungs by qRT-PCR as previously published[29,55]. [A.G.S.] Infectious virus titers in nasal turbinates and lungs were determined by plaque assay on Vero-TMPRSS2 cells as described[59].

(b) Hamster studies.

[A.C.M.B.] Lungs were collected 4 dpi and homogenized in 1.0 mL DMEM, clarified by centrifugation (1,000 x g for 5 min) and stored at -80°C. Nasal washes were clarified by centrifugation (2,000 x g for 10 min) and the supernatant was stored at -80°C. To quantify viral load in lung tissue homogenates and nasal washes, RNA was extracted from 100 µL samples using E.Z.N.A.® Total RNA Kit I (Omega) and eluted with 50 µL of water. Four microliters RNA was used for real-time RT-qPCR to detect and quantify *N* gene of SARS-CoV-2 using TaqMan™ RNA-to-CT 1-Step Kit (Thermo Fisher Scientific) as described[60]. [Y.K.] The virus titers in the nasal turbinates and lungs were determined by plaque assay on Vero E6 cells expressing human TMRPSS2 as previously published[61]. [R.J.W.] RNA was extracted from clarified nasal washes using the Qiagen RNeasy extraction kit (Qiagen, Hilden Germany) following the manufacturer's instructions. Samples were purified on the included columns and

eluted in 50 µL of nuclease free water. PCR was conducted using 4X TaqMan Fast Virus Master Mix (Thermo Fisher) and an *N*-gene primer/probe set.

Plaque assay

Vero-TMPRSS2 or Vero-TMPRSS2-hACE2 cells were seeded at a density of 1×10^5 cells per well in 24-well tissue culture plates. The following day, medium was removed and replaced with 200 µL of material to be titrated diluted serially in DMEM supplemented with 2% FBS. One hour later, 1 mL of methylcellulose overlay was added. Plates were incubated for 72 h, then fixed with 4% paraformaldehyde (final concentration) in PBS for 20 min. Plates were stained with 0.05% (w/v) crystal violet in 20% methanol and washed twice with distilled, deionized water.

Measurement of cytokines and chemokines

Superior and middle lobes of the lungs from K18-hACE2 mice (mock-infected or 3 dpi) were collected, homogenized, and then stored at -80°C. After thawing, lung homogenates were centrifuged at 10,000 x *g* for 5 min at 4°C. Samples were inactivated with ultraviolent light in a clear, U-bottom 96-well plate (Falcon). A murine 26-plex, bead-based Luminex assay (Cat. No. EPXR260-26088-901) was used to profile cytokine and chemokine levels in clarified lung supernatants. The assay was performed according to the manufacturer's instructions, and all incubation steps occurred on an orbital shaker set at 300 rpm. Briefly, 50 µL of clarified lung homogenate supernatant was combined with beads in a lidded, black 96-well plate supplied by the kit and incubated for 30 min at room temperature, and then overnight at 4°C. The next day, the plate was allowed to equilibrate to room temperature for 30 min, washed 3 times with 150 µL/well of 1X Wash Buffer diluted, and then 25 µL/well of 1X Detection Antibody mixture was added for 30 min at room temperature. The plate was washed 3 times, and then 50 µL/well of 1X

Streptavidin-PE solution was added for 30 min at room temperature. After washing 3 times, 120 μL/well of Reading Buffer was added, and the plate was incubated for 5 min at room temperature. Data was acquired on a Luminex 100/200 analyzer (Millipore) with xPONENT software (Version 4.3) and analyzed using GraphPad Prism (Version 8.0) and R (Version 4.0.5).

Micro-CT imaging

Hamsters were inoculated intranasally with 10^3 PFU (in 30 μL) of B.1.1.529 (strain NC928), B.1.617.2 (UW-5250) or PBS. Lungs of the infected animals were imaged by using an in *vivo* micro-CT scanner (CosmoScan FX; Rigaku Corporation, Japan). Under ketamine-xylazine anesthesia, the animals were placed in the image chamber and scanned for 2 min at 90 kV, 88 μA, FOV 45 mm, and pixel size 90.0 μm. After scanning, the lung images were reconstructed by using the CosmoScan Database software of the micro-CT (Rigaku Corporation, Japan) and analyzed by using the manufacturer-supplied software. A CT severity score, adapted from a human scoring system, was used to grade the severity of the lung abnormalities[62]. Each lung lobe was analyzed for degree of involvement and scored from 0–4 depending on the severity: 0 (none, 0%), 1 (minimal, 1%–25%), 2 (mild, 26%–50%), 3 (moderate, 51%–75%), or 4 (severe, 76%–100%). Scores for the five lung lobes were summed to obtain a total severity score of 0–20, reflecting the severity of abnormalities across the three infected groups. Images were anonymized and randomized; the scorer was blinded to the group allocation.

Pathology

[T.S.] Excised animal tissues were fixed in 4% paraformaldehyde in PBS, and processed for paraffin embedding. The paraffin blocks were cut into 3-μm-thick sections and mounted on silane-coated glass slides. Sections were processed for *in situ* hybridization using an RNA scope

2.5 HD Red Detection kit (Advanced Cell Diagnostics, Newark, California) with antisense probe targeting the nucleocapsid gene of SARS-CoV-2 (Advanced Cell Diagnostics). Lung tissue sections were scored for pathology based on the percentage of alveolar inflammation in a given area of a pulmonary section collected from each animal in each group using the following scoring system: 0, no pathological change; 1, affected area (≤10%); 2, affected area (<50%, >10%); 3, affected area (≥50%); an additional point was added when pulmonary edema and/or alveolar hemorrhage was observed.

Reagent availability

All reagents described in this paper are available through Material Transfer Agreements.

Statistical analysis

The number of independent experiments and technical replicates used are indicated in the relevant Figure legends. Statistical analysis included unpaired t tests, Mann-Whitney tests, and ANOVA with multiple correction post-tests.

Reporting summary

Further information on research design is available in the Nature Research Reporting Summary linked to this paper.

Data availability

All data supporting the findings of this study are available within the paper and in the Source Data. There are no restrictions in obtaining access to primary data.

Code availability

No code was used in the course of the data acquisition or analysis.

50 Zang, R. *et al.* TMPRSS2 and TMPRSS4 promote SARS-CoV-2 infection of human small intestinal enterocytes. *Sci Immunol* **5**, doi:10.1126/sciimmunol.abc3582 (2020).

51 Matsuyama, S. *et al.* Enhanced isolation of SARS-CoV-2 by TMPRSS2-expressing cells. *Proc Natl Acad Sci U S A* **117**, 7001-7003, doi:10.1073/pnas.2002589117 (2020).
52 Chen, R. E. *et al.* Resistance of SARS-CoV-2 variants to neutralization by monoclonal and serum-derived polyclonal antibodies. *Nat Med*, doi:10.1038/s41591-021-01294-w (2021).
53 Plante, J. A. *et al.* Spike mutation D614G alters SARS-CoV-2 fitness. *Nature*, doi:10.1038/s41586-020-2895-3 (2020).
54 Gagne, M. *et al.* Protection from SARS-CoV-2 Delta one year after mRNA-1273 vaccination in rhesus macaques coincides with anamnestic antibody response in the lung. *Cell*, doi:10.1016/j.cell.2021.12.002 (2021).
55 Corbett, K. S. *et al.* mRNA-1273 protects against SARS-CoV-2 beta infection in nonhuman primates. *Nat Immunol*, doi:10.1038/s41590-021-01021-0 (2021).
56 Li, Z. *et al.* Generation of transgenic pigs by cytoplasmic injection of piggyBac transposase-based pmGENIE-3 plasmids. *Biology of reproduction* **90**, 93, doi:10.1095/biolreprod.113.116905 (2014).
57 Case, J. B., Bailey, A. L., Kim, A. S., Chen, R. E. & Diamond, M. S. Growth, detection, quantification, and inactivation of SARS-CoV-2. *Virology* **548**, 39-48, doi:10.1016/j.virol.2020.05.015 (2020).
58 Vanderheiden, A. *et al.* CCR2-dependent monocyte-derived cells restrict SARS-CoV-2 infection. *bioRxiv*, doi:10.1101/2021.05.03.442538 (2021).
59 Jangra, S. *et al.* Sterilizing Immunity against SARS-CoV-2 Infection in Mice by a Single-Shot and Lipid Amphiphile Imidazoquinoline TLR7/8 Agonist-Adjuvanted Recombinant Spike Protein Vaccine*. *Angew Chem Int Ed Engl* **60**, 9467-9473, doi:10.1002/anie.202015362 (2021).
60 Chu, D. K. W. *et al.* Molecular Diagnosis of a Novel Coronavirus (2019-nCoV) Causing an Outbreak of Pneumonia. *Clin Chem*, doi:10.1093/clinchem/hvaa029 (2020).
61 Halfmann, P. *et al.* SARS-CoV-2 Interference of Influenza Virus Replication in Syrian Hamsters. *J Infect Dis*, doi:10.1093/infdis/jiab587 (2021).
62 Chung, M. *et al.* CT Imaging Features of 2019 Novel Coronavirus (2019-nCoV). *Radiology* **295**, 202-207, doi:10.1148/radiol.2020200230 (2020).

Acknowledgements This study was supported by grants and contracts from NIH (R01 AI157155 [M.S.D], U01 AI151810 [M.S.D. and A.C.M.B.], 75N93021C00014 (Center for Research on Influenza Pathogenesis and Transmission (CRIPT)) [Y.K. and A.G.S.], HHSN272201400008C [Y.K.], HHSN272201700041I [Z.W.], 75N93020F00001/A38 [Z.W.], P51OD011132 [M.S.S.], R56AI147623 [M.S.S.], HHSN272201400004C [M.S.S.], 75N93021C00017 [M.S.S.], P01 AI060699 [S.P.], R01 AI129269 [S.P.], R01DK130425 [M.S.], 5T32AI007647-22 [L.A.C.] and 75N93019C00051 [M.S.D.], 75N93021C00016 (St. Jude Center of Excellence on Influenza Research and Response (CEIRR)) [R.J.W. and A.C.M.B.]), as well as

grants from Defense Advanced Research Projects Agency (HR0011-19-2-319 0020 [A.G.S.]), the Research Program on Emerging and Re-emerging Infectious Diseases (JP20fk0108412, JP21fk0108615, JP20fk0108472, and JP21fk0108104), a Project Promoting Support for Drug Discovery (JP20nk0101632), the Japan Program for Infectious Diseases Research and Infrastructure (JP21wm0125002) from the Japan Agency for Medical Research and Development (AMED). The Woodruff Health Sciences Center and Emory School of Medicine, Woodruff Health Sciences Center 2020 COVID-19 CURE Award, and the Intramural program of NIAID, NIH [D.C.D., R.A.S., and N.J.S.] also supported this study. The piggyBac vector, pmhyGEMIE-3, was a gift from Dr. Stefan Moisyadi at the University of Hawaii. The Mount Sinai Pathogen Surveillance (E.M.S., H.v.B., V.S.) is supported by institutional school and hospital funds as well as by an option to 75N93021C00014 (A.G.S.). We thank Dr. Randy Albrecht for support with the BSL3 facility and procedures at the Icahn School of Medicine at Mount Sinai, New York.

Author contributions P.J.H., S.I., K.I-H., T.M., M.K., S.M.S., T.L.D., A.J., S.L.F., B.Y., B.W., K.F., M.U., N.N., M.I., R.W., R.U., R.L., Y.L., D.L., J.P.H-O., K.C., K.F., M.P., A.O., L-Y. W., A.B., V.V.E., Z.C., H.U., M.S., T.S., K.C., J.B.C., J.F., T.F., T.J., P.S., J.D., Z.C., G.S., P.W. and L.K. performed the infection experiments in mice and hamsters, titrated virus in tissues, and analyzed pathology. L.A.C. performed the cytokine analysis. R.L., Y.L., D.L. and Z.W. generated human ACE2 hamsters. E.O., J.P.H-O., K.C., K.R.F., A.C.B., D.C.D., P.J.H., G.S., M.G., Y.S-T., and A.R.H. generated, propagated, and/or sequenced viruses. S.L. analyzed the micro-CT images. A.S.G.R. and H.v.B. performed screening and whole virus genome analysis. E.M.S., H.v.B., and V.S. planned the viral surveillance and analyzed data. The PSP study group contributed to the rapid accessioning and transfer of nasopharyngeal swabs, the extraction of

RNA and sequencing allowing for the quick identification of B.1.1.529 in New York City. Y.K., M.S.S., A.G.S., M.S., R.A.S., R.J.W., J.E.O., Z.W., H.U., S.Y., M.I., N.J.S., L.B.T., T.Z., A.C.M.B., and M.S.D. obtained funding, conceived of the study, and supervised research. A.C.M.B., Y.K., and M.S.D. wrote the initial draft, with all other authors providing editorial comments.

Competing interests M.S.D. is a consultant for Inbios, Vir Biotechnology, Senda Biosciences, and Carnival Corporation, and on the Scientific Advisory Boards of Moderna and Immunome. The Diamond laboratory has received funding support in sponsored research agreements from Moderna, Vir Biotechnology, and Emergent BioSolutions. The Boon laboratory has received unrelated funding support in sponsored research agreements from AI Therapeutics, AbbVie Inc., GreenLight Biosciences Inc., and Nano targeting & Therapy Biopharma Inc. M.S.S serves on Advisory boards for Moderna and Ocugen. Y.K. has received unrelated funding support from Daiichi Sankyo Pharmaceutical, Toyama Chemical, Tauns Laboratories, Inc., Shionogi & Co. LTD, Otsuka Pharmaceutical, KM Biologics, Kyoritsu Seiyaku, Shinya Corporatoin, and Fuji Rebio. The A.G.S. laboratory has received unrelated research support from Pfizer, Senhwa Biosciences, Kenall Manufacturing, Avimex, Johnson & Johnson, Dynavax, 7Hills Pharma, Pharmamar, ImmunityBio, Accurius, Nanocomposix, Hexamer, N-fold LLC, Model Medicines, Atea Pharma and Merck. A.G.-S. has paid or equity-based consulting agreements for the following companies: Vivaldi Biosciences, Contrafect, 7Hills Pharma, Avimex, Vaxalto, Pagoda, Accurius, Esperovax, Farmak, Applied Biological Laboratories, Pharmamar, Paratus, CureLab Oncology, CureLab Veterinary and Pfizer, outside of the reported work. A.G.-S. is inventor on patents and patent applications on the use of antivirals and vaccines for the treatment and prevention of virus infections and cancer, owned by the Icahn School of Medicine at Mount

Sinai, New York, outside of the reported work. Icahn School of Medicine at Mount Sinai has filed patent applications relating to SARS-CoV-2 serological assays that list Viviana Simon as co-inventor. S.P. has received unrelated research support from BioAge Laboratories and Autonomous Therapeutics Inc. The remaining authors declare no competing interests.

Additional information
Supplementary information is available for this paper at
Correspondence and requests for materials should be addressed to Adrianus C.M. Boon, Michael S. Diamond and Yoshihiro Kawaoka.
Peer review information *Nature* thanks Emmie de Wit and the other, anonymous, reviewer(s) for their contribution to the peer review of this work.
Reprints and permissions information is available at www.nature.com/reprints.

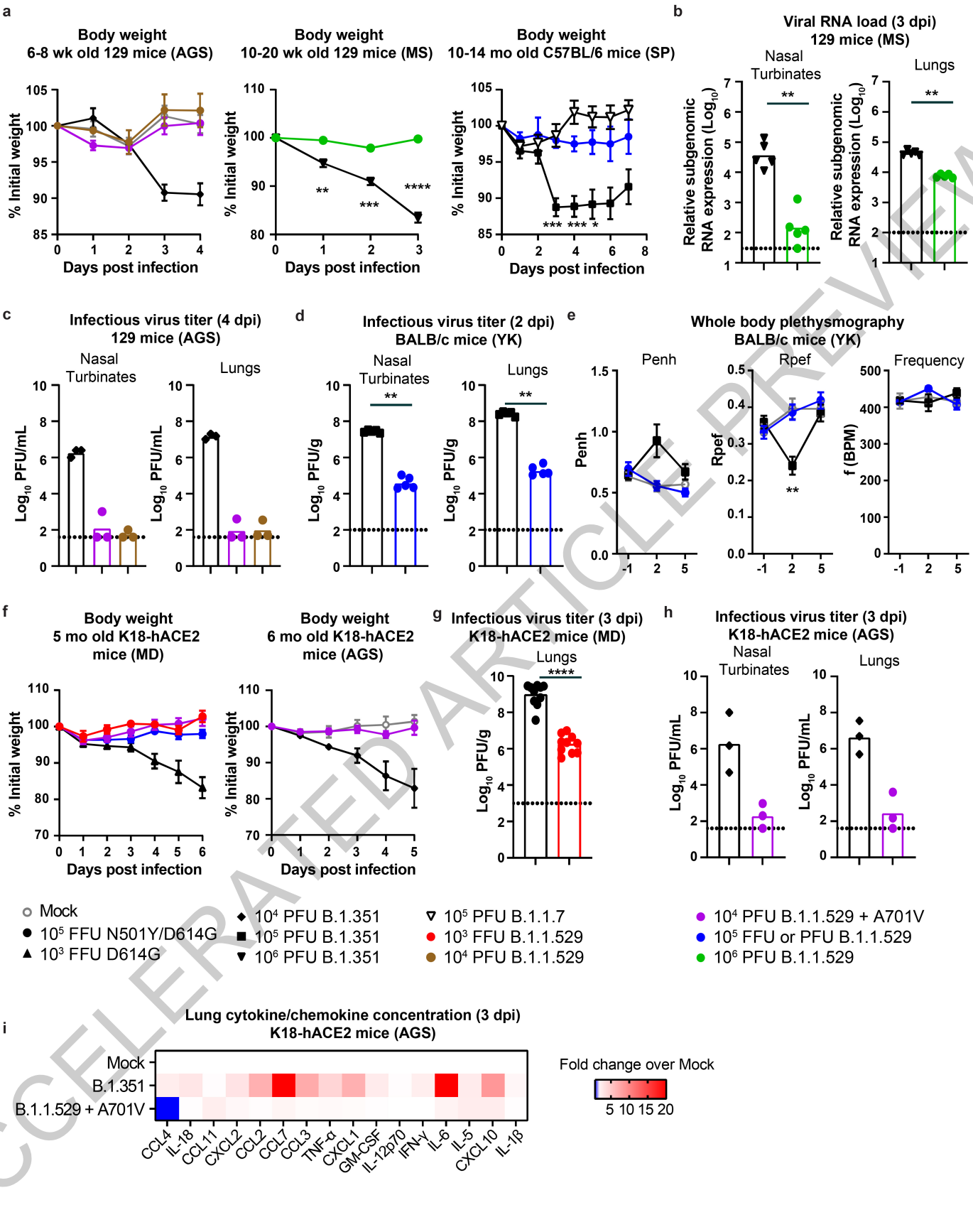

Fig. 1 | See next page for caption.

Fig. 1 B.1.1.529 is less pathogenic in mice. a, *Left*: Weight change in mock-infected 129 mice (n = 4) or 129 mice inoculated with 10^4 (n = 5) PFU of B.1.1.529 + A701V, 10^4 (n = 3) PFU of B.1.1.529, or B.1.351 (n = 3). *Middle*: Weight change in 129 mice inoculated with 10^6 PFU of B.1.1.529 or B.1.351 (n = 5) (** P = 0.0075, *** P = 0.0006, **** P < 0.0001). *Right*: Weight change in C57BL/6 mice inoculated with 10^5 PFU of B.1.1.529 (n = 4), B.1.1.7 (n = 10), or B.1.351 (n = 18). Mean ± SEM. Comparison between B.1.351 and B.1.1.529: * P = 0.0151, *** P = 0.0003 (3 dpi) and 0.0006 (4 dpi). **b,** Nasal turbinates and lung viral RNA levels in 129 mice inoculated with 10^6 PFU of B.1.1.529 or B.1.351 (n = 5) (** P = 0.0079). **c,** Infectious virus in nasal turbinates and lungs of 129 mice inoculated with 10^4 PFU of B.1.1.529 + A701V, B.1.1.529, or B.1.351 (n = 3). **d,** Nasal turbinates and lung virus titers from BALB/c mice inoculated with 10^5 PFU of B.1.1.529 or B.1.351 (n = 5) (** P = 0.0079). **e,** Pulmonary function analysis as measured by whole body plethysmography. Mean ± SEM. Comparison between B.1.617.2 and B.1.351. ** P = 0.0095 (n = 5 each). **f**, *Left:* Weight change in K18-hACE2 mice inoculated with 10^3 (n = 3), 10^4 (n = 6), or 10^5 (n = 3) FFU of B.1.1.529 or WA1/2020 D614G (n = 6). *Right:* Weight change in K18-hACE2 mice inoculated with 10^4 PFU of B.1.1.529 + A701V or B.1.351 (n = 6). Age-matched uninfected mice (n = 4) are controls. Mean ± SEM. **g,** Infectious virus in lungs of K18-hACE2 mice inoculated with 10^3 FFU of WA1/2020 D614G (n = 8) or B.1.1.529 (n = 7). (**** P < 0.0001). **h,** Infectious virus in nasal turbinates and lungs of K18-hACE2 mice inoculated with 10^4 PFU of B.1.1.529 + A701V or B.1.351 (n = 3). **i,** Heat map of cytokines and chemokines in lungs of infected K18-hACE2 mice. The results are from one (**a-f**, and **h-i**) or two (**g**) experiments. The dotted line is the limit of detection (LOD). Statistical analysis (**a**, **e**: two-way ANOVA with multiple comparisons test; **b**, **d, g:** two-tailed Mann-Whitney test) was performed on datasets with four or more data points. See **Supplementary Table 1** for more information.

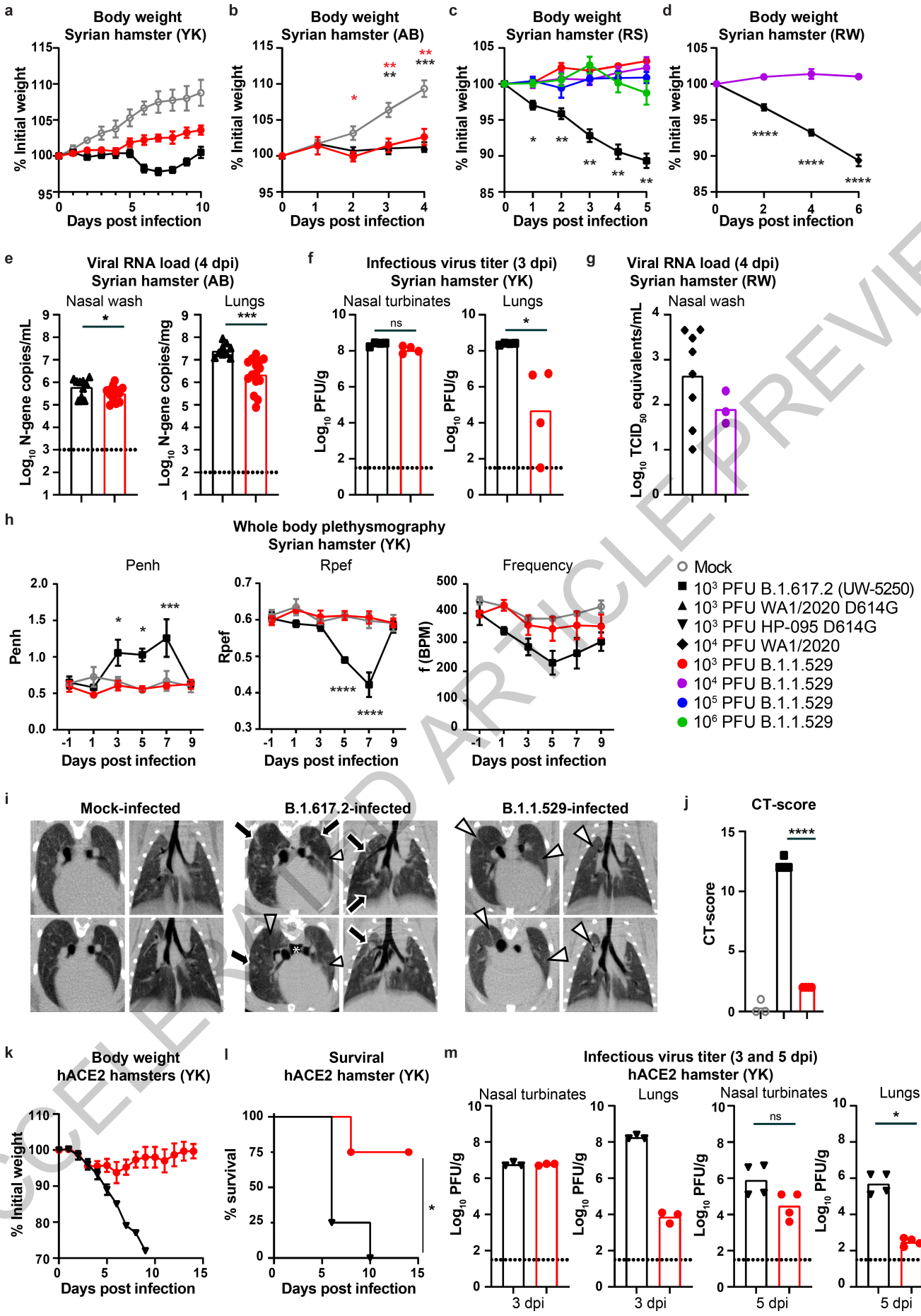

Fig. 2 | See next page for caption.

Fig. 2 B.1.1.529 is less pathogenic in wild-type and hACE2-transgenic Syrian hamsters. a, Weight change in uninfected age-matched Syrian hamsters (n = 3) or in hamsters inoculated with 10^3 PFU of B.1.1.529 or B.1.617.2 (n = 4). Mean ± SEM. **b**, Weight change in uninfected age-matched Syrian hamsters (n = 9) or in hamsters inoculated with 10^3 PFU of B.1.1.529 (n = 10) or WA1/2020 D614G (n = 6). Mean ± SEM. (Red, **P* = 0.0293; Red, ** *P* = 0.0046 and 0.0014; Black, ** *P* = 0.0021; Black, *** *P* = 0.0001). **c**, Weight change in Syrian hamsters inoculated with 10^3, 10^4, 10^5, or 10^6 PFU of B.1.1.529 or 10^3 PFU of B.1.617.2 (n = 4). Mean ± SEM (Comparison between B.1.617.2 and B.1.1.529 [10^3 PFU]; * *P* = 0.0476, ** *P* = 0.0041, 0.0041, 0.0047, and 0.0019, respectively). **d**, Weight change in hamsters inoculated with 10^4 PFU of B.1.1.529 (n = 5) or WA1/2020 (n = 9). Mean ± SEM (****, *P* < 0.0001). **e,** Viral RNA levels in Syrian hamsters inoculated with 10^3 PFU of WA1/2020 D614G or B.1.1.529 (n = 15) (* *P* = 0.015, *** *P* < 0.0003). **f,** Virus titers in Syrian hamsters inoculated with 10^3 PFU of B.1.617.2 or B.1.1.529 (n = 4) (* *P* = 0.0286; ns, not significant). **g,** Nasal wash viral RNA levels in Syrian hamsters inoculated with 10^4 PFU of WA1/2020 (n = 8) or B.1.1.529 (n = 3). **h,** Pulmonary function analysis by whole body plethysmography. Mean ± SEM (Penh and Rpef: comparison between B.1.617.2 and B.1.1.529. * *P* = 0.0263 (3 dpi), * *P* = 0.0186 (5 dpi), *** *P* = 0.0005 (7 dpi), **** *P* < 0.0001) (n = 4). **i**, Micro-CT images of the lungs of mock-infected (n = 3) or B.1.617.2- (n = 4) and B.1.1.529-infected (n = 4) hamsters on 7 dpi. Multifocal nodules (black arrows), ground glass opacity (white arrowheads), and pneumomediastinum (white asterisks) are indicated. **j**, CT score for uninfected hamsters (n = 3) or those inoculated with 10^3 PFU of B.1.617.2 or B.1.1.529 (n = 4). (**** *P* < 0.0001). **k**, Weight change in hACE2-Syrian hamsters inoculated with 10^3 PFU of HP-095 D614G or B.1.1.529 (n = 4). Error bars indicate standard error the mean. **l,** Survival of hACE2-Syrian hamsters after inoculation with 10^3 PFU of HP-095 D614G or B.1.1.529 (n = 4) (* *P* = 0.029). **m,** Infectious virus at 3 and 5 dpi from hACE2-Syrian hamsters inoculated with 10^3 PFU of HP-095 D614G or B.1.1.529; n = 3 (3 dpi), n = 4 (5 dpi). (* *P* = 0.0286; ns, not significant). The results are from one (**a**, **c-d**, and **f-m**) or two to three independent (**b**, and **e**) experiments. Dotted lines represent the LOD. Statistical analysis (**b, c, d, h**: two-way ANOVA with multiple comparisons test; **e**, **j:** two-tailed t test, **f, m**: two-tailed Mann-Whitney test, **l**: log-rank test) was performed on datasets with four or more data points. See **Supplementary Table 1** for more information.

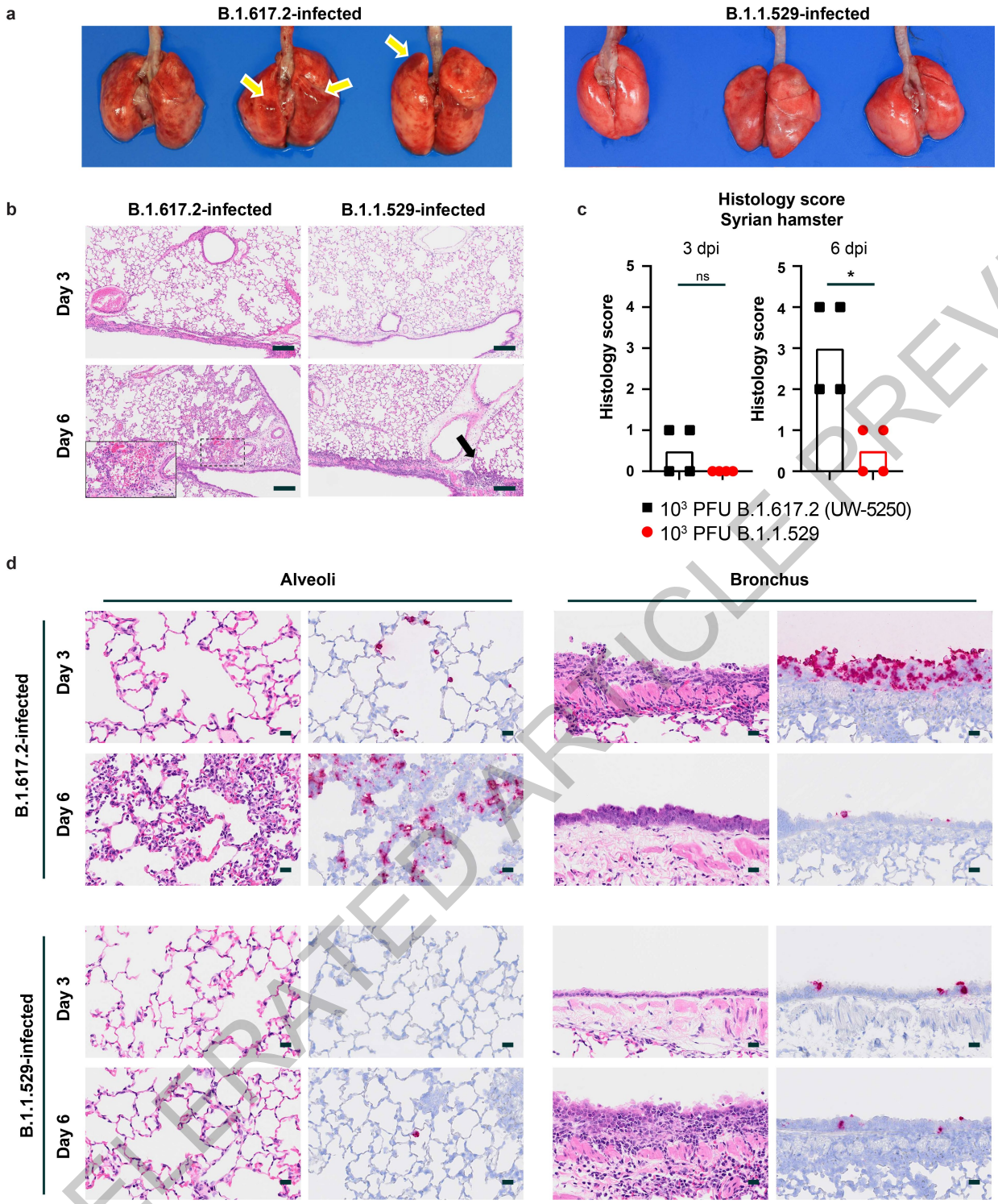

Fig. 3 | See next page for caption.

Fig. 3 Pathological findings in the lungs of SARS-CoV-2 infected Syrian hamsters.

Hamsters were inoculated with 10^3 PFU of B.1.617.2 or B.1.1.529 and sacrificed at 3 and 6 dpi (n = 4). **a**, Macroscopic images of the lungs obtained at 6 dpi. Yellow arrows indicate hemorrhage. **b**, Lung sections obtained from the animals infected with B.1.617.2 or B.1.1.529 at 3 or 6 dpi are shown. Scale bars, 200 μm. Focal alveolar hemorrhage in B.1.617.2-infected animals at 6 dpi is highlighted by dashed lines and shown at higher magnification in the inset (scale bar, 100 μm). Black arrow indicates focal inflammation. **c**, Histopathological score of pneumonia based on the percentage of alveolitis in a given section using the following scoring: 0, no pathological change; 1, affected area (≤10%); 2, affected area (<50%, >10%); 3, affected area (≥50%); an additional point was added when pulmonary edema and/or alveolar hemorrhage was observed. Data are median score ± 95% confidential interval (n = 4; * $P = 0.0286$, ns = not significant; two-tailed Mann-Whitney test). **d**, RNA *in situ* hybridization for SARS-CoV-2 viral RNA. Representative images for the alveoli and bronchi of hamsters infected with B.1.617.2 or B.1.1.529 (n = 4) virus at 3 or 6 dpi are shown. Left panels, alveolar region. Right panels, bronchial region. Scale bars, 20 μm. See **Supplementary Table 1** for more information.

Supplemental Table 1. List of experiments and viruses used by different laboratories

Laboratory	Animal model	Phenotype	Virus detection method	Days post infection	Virus isolates
Kawaoka (YK)	BALB/c mice	Virus titer in Nasal turbinates and Lungs; WBP*	Infectious virus titer	2	B.1.351 (hCoV-19/USA/MD-HP01542/2021) B.1.1.529 (hCoV-19/Japan/NC928-2N/2021)
	Syrian Hamster	Weight loss; Virus titer in Nasal turbinates and Lungs; WBP; CT scan[&]	Infectious virus titer	3	B.1.617.2 (hCoV-19/USA/WI-UW-5250/2021) B.1.1.529 (hCoV-19/Japan/NC928-2N/2021)
	hACE2-transgenic Syrian Hamster	Weight loss; Survival; Virus titer in Nasal turbinates and Lungs	Infectious virus titer	3 and 5	HP-095 (SARS-CoV-2/UT-HP095-1N/Human/2020/Tokyo) B.1.1.529 (hCoV-19/USA/WI-WSLH-221686/2021)
Suzuki (TS)	Syrian Hamster	Histopathology			B.1.617.2 (hCoV-19/USA/WI-UW-5250/2021) B.1.1.529 (hCoV-19/Japan/NC928-2N/2021)
Diamond (MD)	K18-hACE2 transgenic mice	Weight loss; Virus titer in Lungs	RT-qPCR and Infectious virus titer	3	WA1/2020-D614G B.1.1.529 (hCoV-19/USA/WI-WSLH-221686/2021)
Boon (AB)	Syrian Hamster	Weight loss; Virus titer in Nasal wash and Lungs	RT-qPCR	4	WA1/2020-D614G B.1.1.529 (hCoV-19/USA/WI-WSLH-221686/2021)
Seder (RS)	Syrian Hamster	Weight loss	-	-	B.1.1.529 (hCoV-19/USA/GA-EHC-2811C/2021) B.1.617.2 (hCoV-19/USA/PHC658/202)
Garcia-Sastre (AGS)	129 mice	Weight loss; Virus titer in Nasal turbinates and Lungs	Infectious virus titer	4	B.1.1.529 (hCoV-19/USA/NY-MSHSPSP-PV44476/2021) B.1.1.529 (hCoV-19/USA/NY-MSHSPSP-PV44488/2021) B.1.351 (hCoV-19/USA/MD-HP01542/2021)

	K18-hACE2 transgenic mice	Weight loss; Virus titer in Nasal turbinates and Lungs; Cytokine production	Infectious virus titer	3	B.1.1.529 (hCoV-19/USA/NY-MSHSPSP-PV44476/2021) B.1.351 (hCoV-19/USA/MD-HP01542/2021)
Perlman (SP)	C57BL/6 mice	Weight loss	-	-	B.1.1.529 (hCoV-19/USA/GA-EHC-2811C/2021) B.1.351 (hCoV19/20H/501Y.V2) B.1.1.7 (hCoV-19/USA/CA_CDC_5574/2020)
Suthar (MS)	129 mice	Weight loss; Virus titer in Nasal turbinates and Lungs	RT-qPCR	3	B.1.1.529 (hCoV-19/USA/GA-EHC-2811C/2021) B.1.351 (hCoV-19/USA/MD-HP01542/2021)
Webby (RW)	Syrian hamster	Weight loss; Virus titer in Nasal wash	RT-qPCR	4	B.1.1.529 (hCoV-19/USA/GA-EHC-2811C/2021) USA-WA1/2020

* Whole Body Plethysmography, [&] Computerized tomography scan

Supplementary Table 2. Alignment of Key Sequence Changes in B.1.1.529 Omicron Isolates

Gene	NT change	AA change[a]	7263803[b]	7171744[b]	7507055[b]	7908052[b]	7908059[b]
ORF1ab	A2832G	K856R					
ORF1ab	6513_6515 del	SL2083I					
ORF1ab	G8393A	A2710T					
ORF1ab	C10029T	T3255I					
ORF1ab	C10449A	P3395H					
ORF1ab	11288_11296 del	SGF3675 del					
ORF1ab	C14408T	P4715L					
ORF1ab	A18163G	I5967V					
ORF1ab	C21034T	L6924F					
S	C21762T	A67V					
S	21765_21770 del	HV69 del					
S	C21846T	T95I					
S	21987_21995 del	G142D					
S	21987_21995 del	VYY143 del					
S	22194_22196 del	NL211I					
S	22205GAGCCAGAA ins	214EPE ins					
S	G22578A	G339D					
S	C22674T	S371F					
S	T22679C	S373P					
S	C22686T	S375F					
S	G22813T	K417N					
S	T22882G	N440K					
S	G22898A	G446S					
S	G22992A	S477N					
S	C22995A	T478K					
S	A23013C	E484A					
S	A23040G	Q493R					
S	G23048A	G496S					
S	A23055G	Q498R					
S	A23063T	N501Y					
S	T23075C	Y505H					
S	C23202A	T547K					
S	A23403G	D614G					
S	C23525T	H655Y					

S	T23599G	N679K					
S	C23604A	P681H					
S	C23632T	A701V					
S	C23854A	N764K					
S	G23948T	D796Y					
S	C24130A	N856K					
S	A24424T	Q954H					
S	T24469A	N969K					
S	C24503T	L981F					
E	C26270T	T9I					
M	A26530G	D3G					
M	C26577G	Q19E					
M	G26709A	A63T					
N	C28311T	P13L					
N	28362_28370 del	ERS31 del					
N	G28881A, G28882A, G28883C	RG203KR					

[a]Green cells indicate the presence of indicated amino acid substitution in a given isolate; white cells indicate the absence of the substitution in a given isolate.
[b] Isolate identifiers correspond to GISAID sequences

Supplemental Table 3: Cytokine and chemokine concentration in SARS-CoV-2-infected K18-hACE2 transgenic mice

Cytokine/Chemokine	Concentration (mean ± SD (pg/mL))		
	Mock	B.1.351	B.1.1.529 + A701V
IL-10	2.7 ± 0.9	2.0 ± 0.0	3.2 ± 1.5
IL-1β	1.4 ± 0.0	2.3 ± 1.0	1.6 ± 0.2
IL-2	7.8 ± 1.8	4.7 ± 2.6	7.1 ± 5.5
CXCL10	17.8 ± 0.7	155.4 ± 4.7	42.8 ± 28.1
IL-4	1.4 ± 0.0	1.4 ± 0.0	1.4 ± 0.0
IL-5	2.2 ± 0.0	5.4 ± 2.3	5.2 ± 4.5
IL-6	6.7 ± 1.7	452.2 ± 357.8	12.5 ± 7.5
IL-22	13.0 ± 0.0	13.6 ± 1.1	14.2 ± 2.1
IL-9	38.7 ± 15.4	34.3 ± 14.6	56.9 ± 32.0
IL-13	2.9 ± 0.0	2.9 ± 0.0	3.2 ± 0.6
IL-27	2.8 ± 0.2	2.7 ± 0.1	2.6 ± 0.0
IL-23	19.3 ± 6.3	26.8 ± 13.3	37.1 ± 28.2
IFN-γ	2.2 ± 0.0	4.9 ± 2.8	2.2 ± 0.0
IL-12p70	2.3 ± 0.0	2.8 ± 0.5	2.3 ± 0.0
GM-CSF	3.2 ± 0.0	8.0 ± 1.4	3.4 ± 0.4
CXCL1	20.1 ± 1.8	136.8 ± 80.6	25.0 ± 11.5
CCL5	441.3 ± 98.9	453.1 ± 226.1	268.5 ± 165.9
TNF-α	3.7 ± 0.0	14.9 ± 12.0	5.1 ± 2.0
CCL3	8.2 ± 1.2	59.6 ± 7.4	10.4 ± 4.1
CCL7	34.0 ± 26.5	790.0 ± 363.8	57.1 ± 42.7
CCL2	77.8 ± 9.8	535.3 ± 343.0	91.9 ± 47.4
IL-17A	156.3 ± 0.0	156.3 ± 0.0	172.4 ± 28.0
CXCL2	9.5 ± 0.1	27.9 ± 3.4	13.8 ± 4.5
CCL11	175.6 ± 29.6	212.9 ± 75.6	387.7 ± 306.3
IL-18	78.2 ± 34.4	220.2 ± 124.1	89.1 ± 50.6
CCL4	14.9 ± 1.5	34.0 ± 15.4	9.9 ± 3.9

nature research

Corresponding author(s): Michael Diamomd

Last updated by author(s): 01/14/2022

Reporting Summary

Nature Research wishes to improve the reproducibility of the work that we publish. This form provides structure for consistency and transparency in reporting. For further information on Nature Research policies, see our Editorial Policies and the Editorial Policy Checklist.

Statistics

For all statistical analyses, confirm that the following items are present in the figure legend, table legend, main text, or Methods section.

n/a	Confirmed	
☐	☒	The exact sample size (*n*) for each experimental group/condition, given as a discrete number and unit of measurement
☐	☒	A statement on whether measurements were taken from distinct samples or whether the same sample was measured repeatedly
☐	☒	The statistical test(s) used AND whether they are one- or two-sided *Only common tests should be described solely by name; describe more complex techniques in the Methods section.*
☒	☐	A description of all covariates tested
☒	☐	A description of any assumptions or corrections, such as tests of normality and adjustment for multiple comparisons
☐	☒	A full description of the statistical parameters including central tendency (e.g. means) or other basic estimates (e.g. regression coefficient) AND variation (e.g. standard deviation) or associated estimates of uncertainty (e.g. confidence intervals)
☐	☒	For null hypothesis testing, the test statistic (e.g. *F*, *t*, *r*) with confidence intervals, effect sizes, degrees of freedom and *P* value noted *Give P values as exact values whenever suitable.*
☒	☐	For Bayesian analysis, information on the choice of priors and Markov chain Monte Carlo settings
☒	☐	For hierarchical and complex designs, identification of the appropriate level for tests and full reporting of outcomes
☒	☐	Estimates of effect sizes (e.g. Cohen's *d*, Pearson's *r*), indicating how they were calculated

Our web collection on statistics for biologists contains articles on many of the points above.

Software and code

Policy information about availability of computer code

Data collection	No software was used in this study to collect data
Data analysis	Prism 8.0 was used to perform all statistical analysis. xPONENT (version 4.3) and R (version 4.0.5) were used to analyze the cytokine data.

For manuscripts utilizing custom algorithms or software that are central to the research but not yet described in published literature, software must be made available to editors and reviewers. We strongly encourage code deposition in a community repository (e.g. GitHub). See the Nature Research guidelines for submitting code & software for further information.

Data

Policy information about availability of data

All manuscripts must include a data availability statement. This statement should provide the following information, where applicable:

- Accession codes, unique identifiers, or web links for publicly available datasets
- A list of figures that have associated raw data
- A description of any restrictions on data availability

All data supporting the findings of this study are available within the paper and in the Source Data. There are no restrictions in obtaining access to primary data.

Field-specific reporting

Please select the one below that is the best fit for your research. If you are not sure, read the appropriate sections before making your selection.

☒ Life sciences ☐ Behavioural & social sciences ☐ Ecological, evolutionary & environmental sciences

For a reference copy of the document with all sections, see nature.com/documents/nr-reporting-summary-flat.pdf

Life sciences study design

All studies must disclose on these points even when the disclosure is negative.

Sample size	No sample sizes were chosen a priori. All experiments with statistical analysis were repeated at least two independent times, each with multiple technical replicates. Experimental size of cohorts was determined based on prior experience performing studies in animals and with SARS-CoV-2 infection models (PMID: 34846168, 34668780, 32839612, 34140350, and 32571934). The studies were corroborated by independent and parallel experiments by several different groups in the SAVE/NIAID consortia
Data exclusions	No data was excluded.
Replication	All experiments with multiple biological and/or technical replicates are indicated the Figure legends.
Randomization	For animal studies, mice were randomly assigned to treatment groups in an age and sex-matched distribution. All experiments were derived from animal work so no additional randomization was required in downstream analysis.
Blinding	No blinding was performed although several key studies were performed independently by different members of the SAVE consortium. Blinding was not performed because studies were independently corroborated by separate laboratories.

Reporting for specific materials, systems and methods

We require information from authors about some types of materials, experimental systems and methods used in many studies. Here, indicate whether each material, system or method listed is relevant to your study. If you are not sure if a list item applies to your research, read the appropriate section before selecting a response.

Materials & experimental systems

n/a	Involved in the study
☒	☐ Antibodies
☐	☒ Eukaryotic cell lines
☒	☐ Palaeontology and archaeology
☐	☒ Animals and other organisms
☒	☐ Human research participants
☒	☐ Clinical data
☒	☐ Dual use research of concern

Methods

n/a	Involved in the study
☒	☐ ChIP-seq
☒	☐ Flow cytometry
☒	☐ MRI-based neuroimaging

Eukaryotic cell lines

Policy information about cell lines

Cell line source(s)	Vero-TMPRSS2, Diamond and Kawaoka laboratories (not commercially available); Vero-hACE2-TMPRSS2, Graham laboratory, VRC/NIH (available at BEI Resources, NR-54970)
Authentication	These were obtained from academic laboratories and grew and performed as expected. Cells expressing TMPRSS2 and hACE2 were validated using monoclonal antibodies and flow cytometry.
Mycoplasma contamination	All cell lines are routinely tested each month and were negative for mycoplasma.
Commonly misidentified lines (See ICLAC register)	This study did not involve any commonly misidentified cell lines.

Animals and other organisms

Policy information about studies involving animals; ARRIVE guidelines recommended for reporting animal research

Laboratory animals	Heterozygous female K18-hACE2 C57BL/6J mice (strain 2B6.Cg-Tg(K18-ACE2)2Prlmn/J, 5-6 month-old), Male and female 129 mice (strain: 129S2/SvPasCrl or 129S1/SvImJ, 6-8, 10-20, or 31 week-old)), and female C57BL/6 (strain 000664, 10-14 month-old) mice were obtained from The Jackson Laboratory and Charles River Laboratories. Female BALB/c mice (6 week-old) were purchased from

	Japan SLC Inc. Five-to-six-week-old male Syrian Golden hamsters were obtained from Charles River Laboratories, Envigo, or Japan SLC Inc. The K18-hACE2 transgenic hamster line will be described in detail elsewhere (see REF 39; bioRxiv, doi:10.1101/2021.07.26.453840), Mice were housed in groups of 4 to 5; Hamsters were housed alone. Photoperiod = 12 hr on:12 hr off dark/light cycle. Ambient animal room temperature is 70° F, controlled within ±2° and room humidity is 50%, controlled within ±5%.
Wild animals	No wild animals were used in this study.
Field-collected samples	No field collected samples were used in this study.
Ethics oversight	Animal studies were carried out in accordance with the recommendations in the Guide for the Care and Use of Laboratory Animals of the National Institutes of Health. The protocols were approved by the Institutional Animal Care and Use Committee at the Washington University School of Medicine (assurance number A3381–01), University of Wisconsin, Madison (V006426), St. Jude Children's Research Hospital (Assurance number D16-00043), Emory University, University of Iowa (assurance number A3021-01), Icahn School of Medicine at Mount Sinai (PROTO202100007), BIOQUAL, Inc., and the Animal Experiment Committee of the Institute of Medical Science, the University of Tokyo (approval numbers PA19-72 and PA19-75).

Note that full information on the approval of the study protocol must also be provided in the manuscript.